Mukhtar Ahmad, Rizwan Ali, Atiq ur Rehman, Akbar Ali, Ishrat Sultana, Ihsan Ali and Muhammad Asif\*

# Insight into the Structural, Electrical, and Magnetic Properties of Al-Substituted BiFeO<sub>3</sub> Synthesised by the Sol-Gel Method

https://doi.org/10.1515/zna-2019-0283 Received September 5, 2019; accepted January 8, 2020; previously published online February 7, 2020

Abstract: Multiferroics with chemical formula  $BiAl_xFe_{1-x}O_3$  (x = 0, 0.1, 0.2, and 0.3) and substituted by Al are synthesised using sol-gel auto-combustion. The materials are sintered at 500 °C for 5 h. In the ongoing study, the crystal structure of  $BiAl_xFe_{1-x}O_3$  was investigated by X-ray diffraction. After confirming the rhombohedral single-phase crystal structure, various characterisation techniques, such as scanning electron microscopy (SEM), energy-dispersive X-ray (EDX) spectroscopy, elemental mapping images, electrical properties, Fourier transform infrared spectroscopy, and vibrating sample magnetometry (VSM), were used to investigate the synthesised samples. The grain size estimated from SEM images decreased as Al contents increased. Elemental composition was confirmed by EDX spectra. Direct current electrical resistivity increased whereas drift mobility decreased with increasing Al contents. The VSM results of Al-doped BiFeO<sub>3</sub> (BFO) demonstrate that BFO crystals with size >60 nm show anti-ferromagnetic behaviour, which is evident in the present study. The increase in Al doping results in an increase in coercivity, as grain size and coercivity are inversely related with each other. This is because of the replacement of Fe<sup>3+</sup> by Al<sup>3+</sup> ions, which weakens the sub-lattice interactions. It has been observed

\*Corresponding author: Muhammad Asif, Department of Physics, COMSATS University Islamabad, Lahore Campus, 54000 Lahore, Pakistan, E-mail: drmuhammadasif@cuilahore.edu.pk
Mukhtar Ahmad, Rizwan Ali, Akbar Ali and Ishrat Sultana:
Department of Physics, COMSATS University Islamabad, Lahore Campus, 54000 Lahore, Pakistan
Atiq ur Rehman: Department of Physics, COMSATS University Islamabad, Lahore Campus, 54000 Lahore, Pakistan; and Department of Natural and Social Sciences, Sharif College of Engineering and Technology, Lahore, Pakistan
Ihsan Ali: Government Post Graduate College, Toba Tek Singh,

Pakistan

that BFO materials with such parameters are favourable for ferroelectric random access memories where data can be written electrically and read magnetically.

**Keywords:** Al Substitution; BiFeO<sub>3</sub>; Ferroelectric Random Access Memories; M–H Loops; Sol–Gel Auto-Combustion.

#### 1 Introduction

The family of materials that yield ferroelectric, ferromagnetic, antiferromagnetic, and ferroelastic effects simultaneously in the same material are termed as multiferroics, as they possess different ferroic characteristics [1]. In these materials, magnetic and electric phase transitions are strong due to magnetoelectric effects. At low temperatures, multiferroics show multiferroicity in the form of a single phase, and in composite form, these materials exhibit magnetostrictive properties and piezoelectricity. Basically, there are two requirements for multiferroics. First is the coexistence of magnetic and electric dipoles. Second is the coupling between different order parameters and simultaneous violation of space and time inversion [2]. BiFeO<sub>3</sub> (BFO) is promising in this regard due to coupling between ferroelectric and magnetic ordering at room temperature, leading to room temperature devices. BFO is a smart material due to its multiferroic properties, i.e. ferroelectricity with high Curie temperature ( $T_C = 820-850$  °C) [3, 4] and antiferromagnetic properties under Néel temperature ( $T_N = 350-380$  °C) [5, 6]. BFO shows antiferromagnetic G-type spin configuration [7]. Multiferroic materials have attracted great attention due to their potential applications in multifunctional devices [8, 9]. Since the discovery of BFO in 1960, bismuth ferrite powders have been prepared by the solid-state, mechano-chemical, solution chemistry, hydro-thermal, sono-chemical, and sol-gel methods [10]. These methods require high-temperature treatments at >800 °C [11]. To get nanosized samples avoiding bismuth volatilisation, low-temperature synthesis methods are being developed progressively. Among the various solution-based methods for synthesising BFO nanoparticles, we chose sol-gel auto-combustion due to easy control of chemical composition and relatively low sintering temperature, preventing bismuth volatilisation. Bismuth ferrite has a rhombohedral distorted perovskite structure with space group R3c and general chemical formula ABO3 [12]. BFO is considered a promising candidate for magnetic storage or in the applications of spintronic devices [13]. However, leakage current due to oxygen vacancies or impurities is the major problem in BFO [14]. The main reasons of leakage current in BFO are oxygen vacancies and Fe<sup>2+</sup>. Oxygen vacancies are due to Bi<sup>3+</sup>, and Fe<sup>3+</sup> reduction is the cause of Fe<sup>2+</sup>. The aim of doping in BFO is to decrease leakage current [15]. The most studied room temperature BFO is doped with different ions to increase the electric, dielectric, and magnetic properties [16]. In BFO, A site cation is responsible for ferroelectricity and B site cation is responsible for magnetism. Both substitutions or even one substitution in BFO can enhance the electrical and magnetic properties for many purposes [17]. Magnetisation in BFO relies on the radius of doping cation at Bi site. Co doping of Ca<sup>2+</sup> and Ba<sup>2+</sup> alkaline earth metals affects the characteristics of BFO nanoparticles [18]. Rana and Singh studied pure and Ni-substituted ZnO nanoparticles for magnetic and optical properties. Scanning electron microscopy (SEM) images revealed the spherical nanocrystalline structure of the prepared nanoparticles. Optical properties with Ni substitution resulted in blue shift in absorption edge contrary to intrinsic ZnO nanoparticles. Antibacterial activity was enhanced with Ni substitution and sunlight exposure from 40 to 45 µg [19]. Rana et al. and Singh et al. studied the effect of Co doping on ZnO and Fe-ZnO nanoparticles. Co doping changed the diamagnetic behaviour of prepared ZnO nanoparticles into ferromagnetic behaviour. Co-doped ZnO nanoparticles resulted in enhanced antimicrobial activity. Saturation magnetisation increased with Co doping in case of Fe-ZnO nanoparticles [20, 21].

In previous studies, Al<sup>3+</sup> substitution resulted in increased electrical resistivity, hence decreasing the saturation magnetisation and dielectric losses. These developments can be beneficial to enhance the microwave-absorbing properties of ferrite materials [22, 23]. Moreover, Al<sup>3+</sup> ion substitution prevents grain growth and enhances the mechanical strength of the prepared ferrites. Therefore, it seemed reasonable to investigate Al-substituted BFO at Fe<sup>3+</sup> sites synthesised by using the sol–gel (auto-combustion) method in order to alter the different electrical and magnetic properties to use them for different technological and high-frequency applications where low eddy current losses are desired.

# 2 Experimental

#### 2.1 Sample Preparation

Nanocrystalline powders of BiAl<sub>x</sub>Fe<sub>1-x</sub>O<sub>3</sub> (x = 0.0, 0.1, 0.2, and 0.3) were synthesised by using the sol-gel (auto-combustion) method. First, the solution was prepared by dissolving analytical grade  $Bi(NO_3)_3 \cdot 5H_2O$ ,  $Fe(NO_3)_3 \cdot 9H_2O$ ,  $Al(NO_3)_3 \cdot 9H_2O$ , and  $C_6H_8O_7 \cdot H_2O$ in deionised water according to the stoichiometric ratios. Citric acid was used as a chelating or igniting agent. The ratio of citric acid to metal nitrates was set as 1:1. Thereafter, the solution was placed on a hot plate magnetic stirrer while being heated at about 70-80 °C and continuously stirred by the magnetic stirrer until the solution was transformed into a dried gel. When the solution in beaker was left almost 100 mL, then ammonium hydro-oxide was added drop by drop in the mixture to maintain its pH neutral. After 8-10 h, the dried gel was ignited and converted into fluffy powder. As a result, a feathery nanoferrite powder is obtained by blazing the gel through a self-burning process. The synthesised powder is placed into drying oven at 120 °C for 24 h. After synthesising, the materials were crushed for 10 min by use of agate mortar and pestle. The crushed powder was placed into furnace by adjusting its temperate to 500 °C for at least 5 h to sinter the materials. In sintering, the atoms are diffused across the particle boundaries, in order to increase the crystallinity. Thereafter, the material was ready for characterisation.

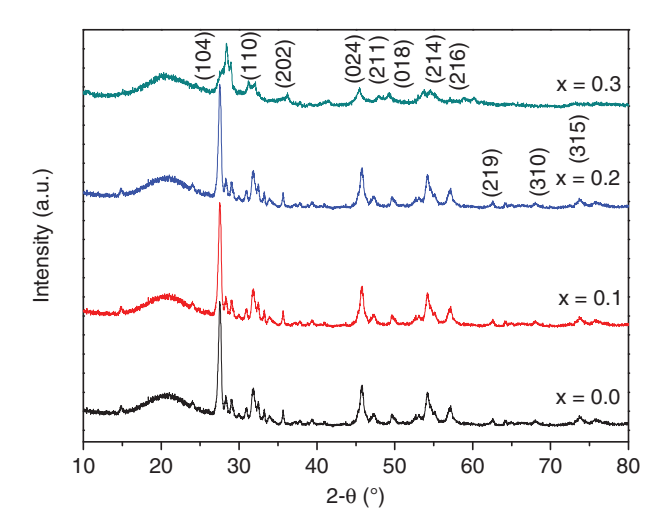
#### 2.2 Characterisation Techniques

The purposed phase of these ferrites was confirmed using a Bruker axis D8 diffractometer with Cu–Ka ( $\lambda=1.54~{\rm \AA}$ ) radiation while operating at 40 kV and 30 mA in the 20 range of 15–80°. The scan step was 0.2°/s during these measurements. The microstructure and grain size was estimated by a field emission scanning electron microscope (Philips XL30SFEG). In addition, the elemental composition of some representative samples was also evaluated using energy-dispersive X-ray (EDX) spectrometry. Room temperature direct current (DC) electrical resistivity was measured using a two-point probe method after converting the powder in round-shaped pellets. Fourier transform infrared (FTIR) analysis was carried out using Shimadzu 8400S IR spectrometer by the KBr pellet method. The room temperature magnetic properties were measured using a vibrating sample magnetometer (LakeShore M-7407).

## 3 Results and Discussion

#### 3.1 Structural Analysis

Figure 1 shows the X-ray diffraction (XRD) patterns of  $BiAl_xFe_{1-x}O_3$  (x=0.0, 0.1, 0.2, and 0.3) samples prepared using sol–gel (auto-combustion). These patterns were compared with the standard patterns of the same compound having Joint Committee on Powder Diffraction Standards card no. 01-086-1518. It can be seen from these patterns that all samples exhibited a single-phase



**DE GRUYTER** 

**Figure 1:** XRD patterns of Al-substituted BiAl<sub>x</sub>Fe<sub>1-x</sub>O<sub>3</sub> (x = 0.0, 0.1,0.2, and 0.3) samples.

rhombohedral crystal structure and that there was no extra peak of any impurity phase. This confirms that Al has been successfully substituted in the BFO lattice.

The lattice constants (a and c) were calculated for all samples by using the given formula and are listed in Table 1.

$$\sin^2 \theta = \frac{\lambda^2}{3a^2} \Big( h^2 + k^2 + hk \Big) + \frac{\lambda^2 l^2}{4c^2}.$$
 (1)

It is seen that the values of lattice constants were smaller for Al-substituted samples in comparison with the unsubstituted samples and unit cell volume (V) decreased with increasing Al contents in the BFO lattice.

This can be explained on the basis of the dissimilarity in ionic radii of Fe<sup>3+</sup> and Al<sup>3+</sup>. In this case of BiAl<sub>x</sub>Fe<sub>1-x</sub>O<sub>3</sub> (x = 0.0, 0.1, 0.2, and 0.3), bigger Fe<sup>3+</sup> (0.67 Å) ions are replaced by lesser Al<sup>3+</sup> (0.51 Å); hence, a reduction in lattice constants and unit cell volume is expected [24]. The volume of unit cell and X-ray density were calculated by the following formulae [2]:

$$V = a^2 c, (2)$$

$$D_X = ZM/N_AV, (3)$$

**Table 1:** Variation of structural parameters  $(a, c, V, \text{ and } D_x)$  as a function of Al substitution.

x	a (Å)	c (Å)	V (Å) <sup>3</sup>	$D_x$ (g/cm <sup>3</sup> )
0.0	5.597	13.986	483.131	6.46
0.10	5.517	13.901	423.108	7.30
0.20	5.521	13.887	423.295	7.22
0.30	5.501	13.904	420.748	7.20

where M is molar mass, Z is number of formula units in a unit cell, V is volume of unit cell, and  $N_A$  is Avogadro's number. The value of Z is equal to 6 because of the R3c space group [3]. Commonly, the crystallite size decreases with enlarging substituents with smaller ionic radii because of mismatch in the size of host and doping cation, leading to local structure disorder [25] and alteration of structural parameters such as a, c, and V. Furthermore, the value of the X-ray density of Al-substituted samples was in the range of 7.30–7.20 g/cm<sup>3</sup>, which is in good agreement with the previous reported values for the same structure [26].

#### 3.2 Grain Size and Morphology

Figure 2 shows the SEM images of clean and Al-doped BFO samples. It can be seen that the grain size decreased with increase in Al doping. This is because of the formation of aluminium oxides at the given boundaries, which stopped grain growth [27]. The surface structure of the samples was dense and non-uniform. Samples had little grain and grain borders, whereas with doped Al, diffuse grain boundaries were observed. Furthermore, the grain size of doped samples was decreased (Tab. 2) with substitution of Al [28]. The decrease in the grain size may be recognised to the covered up oxygen vacancy as a result of doping, that is oxygen vacancies moving during the sintering procedure, which facilitate grain growth [29]. In addition, it has been discussed in XRD analysis that Al doping causes the shrinkage of the unit cell, and it has been reported earlier that shrinkage in unit cell is directly related to the grain size [30].

#### 3.3 Elemental Composition

EDX microanalysis is carried out at working voltage to confirm the content of doping agent in  $BiAl_xFe_{1-x}O_3$ . The location of peaks guide the classification of elements, and the peak height helps in the quantification of the concentration of every element in the sample. In the present study, the elemental composition of the synthesised series was calculated by using EDX, and the suitability of replacing Al instead of Fe in the mixture was assessed. The EDX spectra (Fig. 3) of  $BiAl_xFe_{1-x}O_3$  (x = 0.0, 0.1, and 0.3) for these samples revealed the presence of Bi, Al, O, and Fe, and their contents were in close agreement with the elemental compositions of the dissolved reactants, thus confirming that aluminium ions replaced iron ions in the lattice structure [22]. Every peak was exclusive for all atoms and corresponded to each element. This gives the confirmation

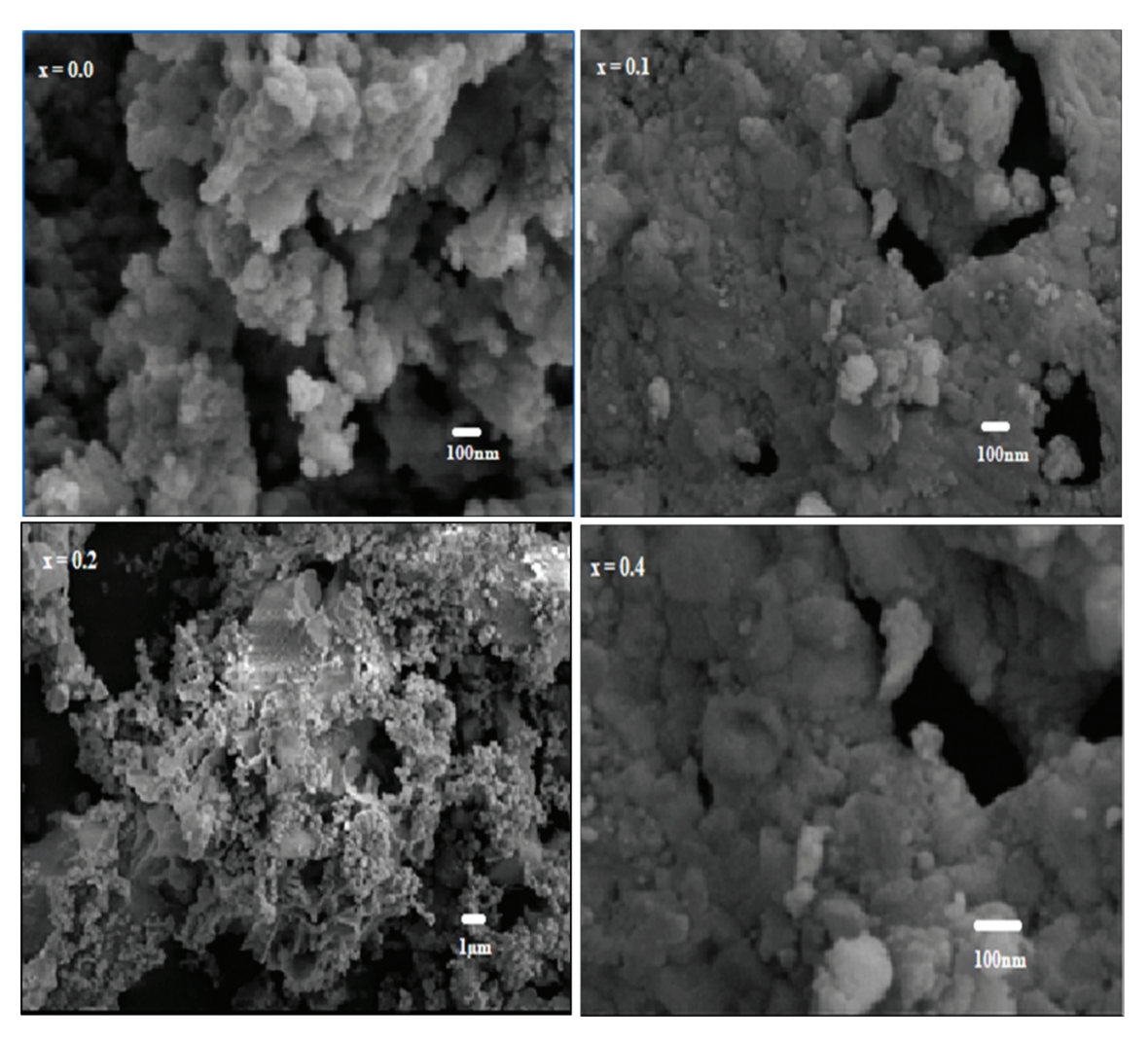


**Figure 2:** SEM images of Al-substituted BiAl<sub>x</sub>Fe<sub>1-x</sub>O<sub>3</sub> (x = 0.0, 0.1, 0.2, and 0.3) samples.

**Table 2:** Variation of grain size vs. Al contents (x).

x	Grain size (nm)	
0.0	73	
0.10	64	
0.20	66	
0.30	58	

of the soluble materials, and no impurity was observed, which matched the XRD results that all samples are single phase with a rhombohedral crystal structure [31]. Each element has unique peaks and energy. EDX is used for both qualitative (element types) and quantitative analyses.

### 3.4 Elemental Mapping

Figure 4 shows the elemental mapping images of an Alsubstituted  $BiAl_xFe_{1-x}O_3$  (x=0.0) sample. The elemental mapping images of  $BiAl_xFe_{1-x}O_3$  were recorded to study

the distribution of elements in the nanostructures. These images showed that Bi, Fe, and O were uniformly distributed in the BFO solution. The density of the particles was the same throughout the material [32].

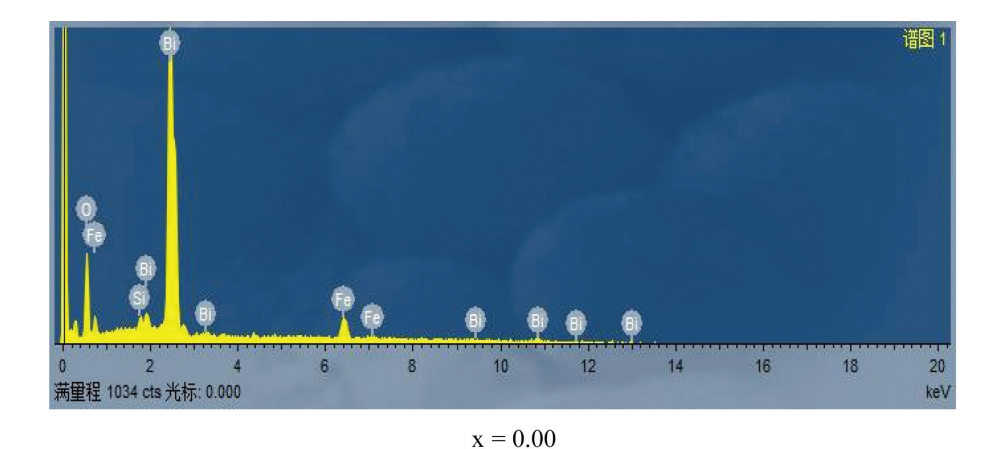
#### 3.5 Electrical Properties

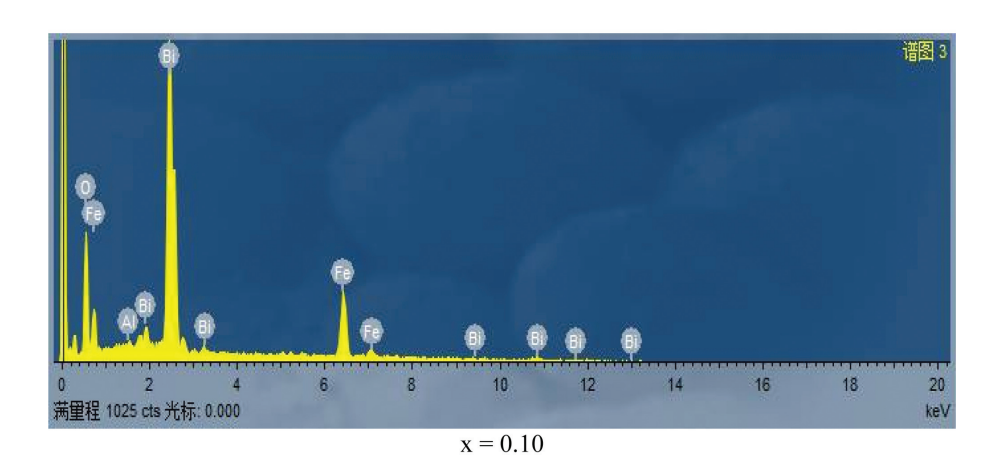
Room temperature DC electrical resistivity ( $\rho_{dc}$ ) can be calculated using the given formula [22]:

$$\rho_{dc} = \frac{RA}{t},\tag{4}$$

where R, A, and t in (4) represent resistance, area, and thickness of the pellet.

Many factors such as microstructure homogeneity, chemical composition, site occupancy of substituted ions, particle size, porosity, and crystal structure affect the resistivity of ceramic materials [33]. In these materials, greater electron hopping between ferrous (Fe<sup>2+</sup>) and ferric (Fe<sup>3+</sup>)





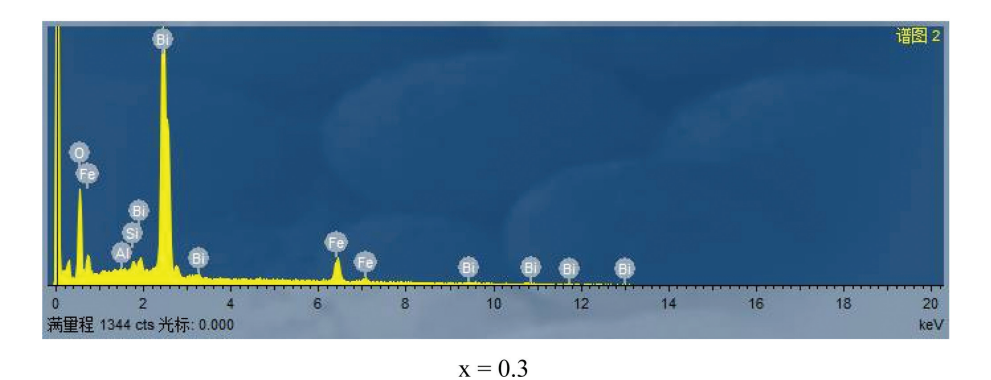
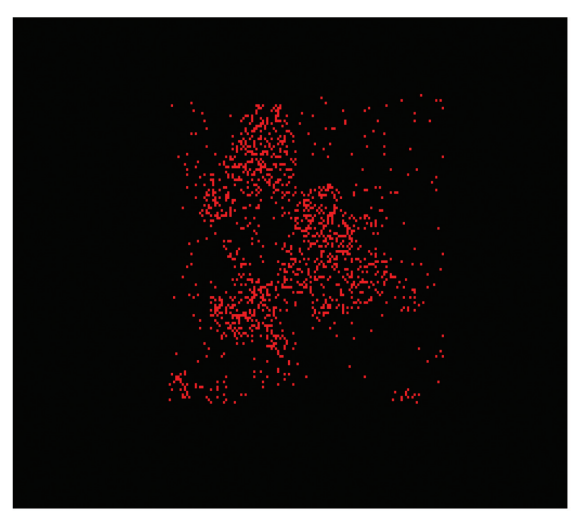
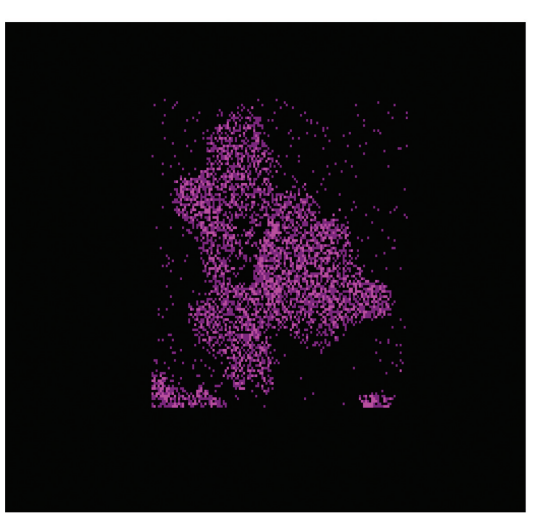


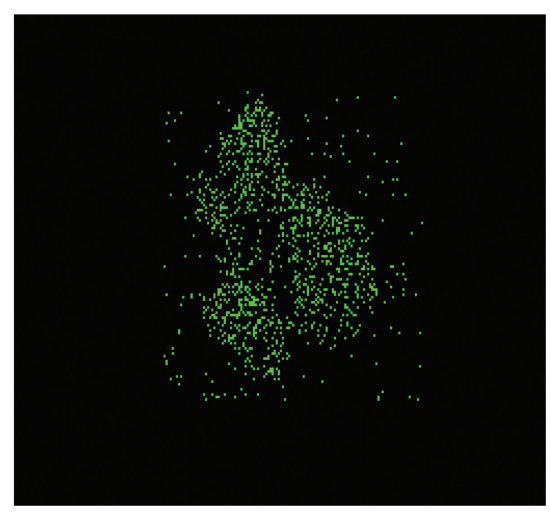
**Figure 3:** EDX spectra of Al-substituted BiAl<sub>x</sub>Fe<sub>1-x</sub>O<sub>3</sub> (x = 0.0, 0.1, and 0.3) samples.

ions at the octahedral sites results in greater conductivity and vice versa. The electrical resistivity of the unsubstituted (x = 0.0) sample was found to be lower than that of the Al-substituted samples (Tab. 3). The minimum value was 8.5  $\times$  10<sup>7</sup>  $\Omega$ -cm at x = 0.0 which increased about four folds to maximum of 7.38  $\times$  10<sup>10</sup>  $\Omega$ -cm at x = 0.3. Substituted Al ions possess an octahedral site preference [34]. Consequently, they replace Fe<sup>3+</sup> ions at these sites. As the percentage of Al increases from 0 % to 30 %, the concentration of Al ions increases at the octahedral sites and that of Fe<sup>3+</sup> ions decreases. This results in lesser hopping of ferrous and ferric ions, as the hopping is proportional to their concentration at the octahedral sites. The Maxwell-Wagner model proposes that low resistive grains are surrounded by resistive grain boundaries. The Al ions can accumulate at the grain boundaries, which are resistive in nature [35]. Increased Al concentration will result in more Al ion accumulation. This decrease in hopping rate and Al ion accumulation results in higher resistivity for Al-substituted samples.



0 Ka1





Bi Ma1 Fe Ka1

**Figure 4:** Elemental mapping images of Al-substituted BiAl<sub>x</sub>Fe<sub>1-x</sub>O<sub>3</sub> (x = 0.0) sample.

**Table 3:** Resistivity ( $\rho$ ), number of charge carriers (n), and drift mobility ( $\mu_d$ ) of BiAl<sub>x</sub>Fe<sub>1-x</sub>O<sub>3</sub> at x=0.0, 0.1, 0.2, and 0.3.

x	ρ (Ω-cm)	n (cm <sup>-3</sup> )	$\mu_d  imes 10^{-13} \ (cm^2V^{-1}s^{-1})$
0.0	$8.5 \times 10^{7}$	$2.69 \times 10^{22}$	3.13
0.1	$4.34\times10^8$	$4.56\times10^{22}$	2.88
0.2	$1.15\times10^{9}$	$7.13 \times 10^{22}$	2.56
0.3	$7.38 \times 10^{9}$	$8.62\times10^{22}$	2.48

The drift mobility  $(\mu_d)$  of the electrons for the given materials can be calculated using the following formula:

$$\mu_{d} = \frac{\sigma}{ne} \tag{5}$$

In (5),  $\sigma$  is conductivity while n and e represent electron concentration and electric charge, respectively. The

electron (charge) concentration can be calculated using the following formula:

$$n = \frac{N_A d_B P_{Fe}}{M},\tag{6}$$

where  $N_A$  is Avogadro's number,  $d_B$  is bulk density, M is molecular mass, and  $P_{Fe}$  is iron atom concentration as determined by EDX analysis.

The drift mobility of the given samples decreased with increasing Al substitution. The maximum  $\mu_d$  was  $3.13 \times 10^{-13}$  cm<sup>2</sup> V<sup>-1</sup> s<sup>-1</sup> (x=0.0), which decreased to a minimum value of  $2.48 \times 10^{-13}$  cm<sup>2</sup> V<sup>-1</sup> s<sup>-1</sup> (x=0.3). This decrease in drift mobility is attributed to the decrease in Fe<sup>3+</sup> ions at octahedral sites with Al substitution resulting in a low hopping rate.

#### 3.6 FTIR Study

The Fourier spectra are important for analysing the stretching produced due to absorption of water, nitrate ions, and metal-ion interactions. The FTIR spectra of  $BiAl_xFe_{1-x}O_3$  at x = 0.2 is shown in Figure 5 with wave number varying from 4000 to 500 cm<sup>-1</sup>. The absorption peaks at 1400 and 820 cm<sup>-1</sup> were due to absorption of nitrate ions. The Fe-O and O-Fe-O bond stretching are responsible for absorption peaks appearing at 589 and 529 cm<sup>-1</sup>, respectively. These results are in agreement with characteristic absorption bands already observed for BFO [36]. Quantities such as  $V_t$ ,  $V_o$ ,  $K_t$ , and  $K_o$  were calculated for characteristic absorption bands and listed in Table 4.

#### 3.7 Magnetic Measurements

The magnetic-hysteresis (M-H) loops for  $BiAl_xFe_{1-x}O_3$ at x = 0.0, 0.1, 0.2, and 0.3 are shown in Figure 6 with magnetic field varying between -20,000 and 20,000 Oe. The obtained magnetic parameters for all samples are listed in Table 5. It is well known that BFO crystals with size >60 nm show anti-ferromagnetic behaviour [37], which is evident in the present study. Such materials show enhancement in magnetisation due to changes in

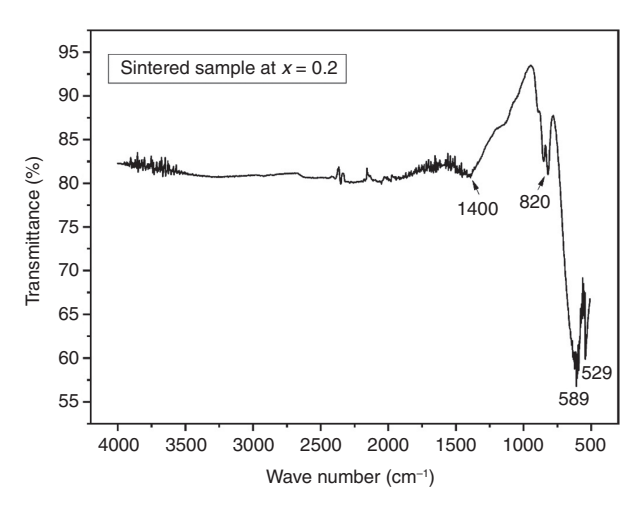
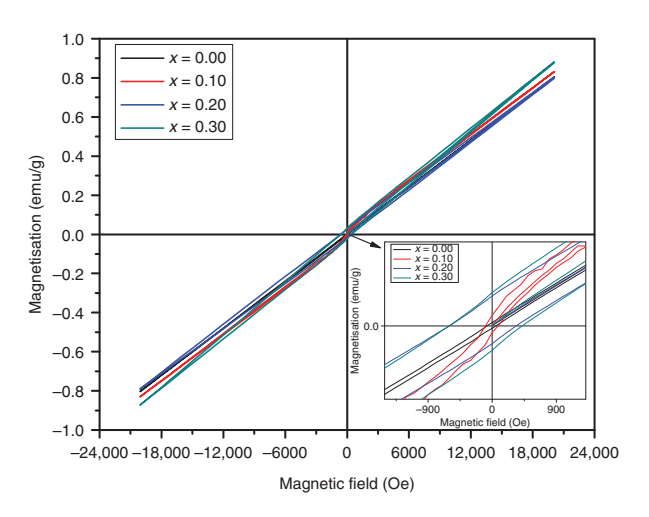


Figure 5: FTIR spectrum of Al-substituted BiAl<sub>x</sub>Fe<sub>1-x</sub>O<sub>3</sub> (x = 0.2) sample.

**Table 4:** Values of  $V_o$ ,  $V_t$ ,  $K_t$ , and  $K_o$  for unsintered BiFeO<sub>3</sub> at x = 0.2.

Vibrational studies of sample	$V_t$ (cm $^{-1}$ )	$V_o$ , (cm $^{-1}$ )	$K_t  imes 10^5$ (dyne/cm)	$K_o  imes 10^5$ (dyne/cm)
Sintered	589.69	529.79	5.515	2.56



**Figure 6:** M-H loops for Al-substituted BiAl<sub>x</sub>Fe<sub>1-x</sub>O<sub>3</sub> (x = 0.0, 0.1,0.2, and 0.3) samples. Inset shows the low field coercivity.

**Table 5:** Magnetisation (M), magnetic remanence ( $M_r$ ), and coercivity  $(H_c)$  of BiAl<sub>x</sub>Fe<sub>1-x</sub>O<sub>3</sub> at x = 0.0, 0.1, 0.2, and 0.3.

x	Magnetisation at 20 kOe (M) (emu/g)	Magnetic remanence (M <sub>r</sub> ) (emu/g)	Coercivity $(H_c)$ (Oe)
0.0	0.797	0.003	70.40
0.1	0.830	0.01	93.95
0.2	0.803	0.028	601.55
0.3	0.878	0.031	603.74

particle size [38]. The minimum value of magnetisation was 0.797 emu/g for the unsubstituted sample and a maximum value of 0.878 emu/g was observed at x = 0.3 for the substituted sample. This is attributed to blocking of antiferromagnetism with reduction in particle size along with the meaningful contribution from anisotropic stresses and spin decompensation on the nanoparticle surface [39]. The magnetic remanence represents the quantity of magnetisation left in the material, when applied magnetic field is nullified. The remanent magnetisation increased from 0.003 to 0.031 emu/g for the unsubstituted and Alsubstituted (x = 0.3) samples. This is due to the nearly distorted spin cycloid structure [40]. The coercivity of the prepared samples increased from 70.40 Oe for x = 0.0to a maximum of 603.74 for x = 0.3. Changes in Fe and O vacancies result in an increase or decrease in coercivity [41]. Moreover, it has also been observed in XRD and SEM analyses that grain size decreases with Al substitution in the BFO lattice, which enhances the coercivity of the prepared samples as both grain size and coercivity are inversely related with each other. It has been observed earlier that BFO materials with such parameters are favourable for ferroelectric random access

memories, where data can be written electrically and read magnetically.

## 4 Conclusion

Single-phase  $BiAl_xFe_{1-x}O_3$  (x = 0.0, 0.1, 0.2, and 0.3) samples were successfully prepared using sol-gel autocombustion. The rhombohedral single-phase structure was confirmed by XRD analysis. Values of lattice constants were found to be smaller for Al-substituted samples in comparison with the unsubstituted sample, and the unit cell volume decreased with increasing Al contents in the BFO lattice. The morphology of the samples was dense and non-uniform. The grain size decreased with increasing Al doping. The elemental mapping investigation clearly showed that the distribution of the elements was uniform in the sample. The FTIR spectrum of the sample showed Fe-O and Bi-O bond stretching in the range of 500-600 cm<sup>-1</sup>. The increase in Al substitution resulted in increase in coercivity due to the replacement of Fe<sup>3+</sup> by  $Al^{3+}$  ions, weakening the sub-lattice interactions.

# References

- [1] D. I. Khomskii, I. Magnetism Magnetic Mater. 306, 1 (2006).
- [2] E. Mostafavi, A. Ataie, M. Ahmadzadeh, M. Palizdar, T. P. Comyn, et al., Mater. Chem. Phys. 162, 106 (2015).
- [3] C. Michel, J.-M. Moreau, G. D. Achenbach, R. Gerson, and W. J. James, Solid State Commun. 7, 701 (1969).
- [4] V. Isupov and A. Skaya, Sov. Phys. Solid State 2, 2651
- [5] G. Smolenskii, V. Yudin, E. Sher, and Y.E. Stolypin, Sov. J. Exp. Theor. Phys. 16, 622 (1963).
- [6] J.-M. Moreau, C. Michel, R. Gerson, and W. J. James, J. Phys. Chem. Solids 32, 1315 (1971).
- [7] D.-C. Jia, J.-H. Xu, H. Ke, W. Wang, and Y. Zhou, J. Eur. Ceram. Soc. 29, 3099 (2009).
- [8] G.-C. Xu, W. Zhang, X.-M. Ma, Y.-H. Chen, L. Zhang, et al., J. Am. Chem. Soc. 133, 14948 (2011).
- [9] S. Wei, Y. Liu, H. Tian, H. Tong, Y. Liu, et al., J. Magnetism Magnetic Mater. 377, 419 (2015).
- [10] M.-G. Ma and J.-F. Zhu, Recent Patents Nanotechnol. 4, 164
- [11] B. Baruwati, D. K. Kumar, and S. V. Manorama, Sens. Actuators B Chem. 119, 676 (2006).
- [12] Y. Inaguma, M. Yoshida, and T. Katsumata, J. Am. Chem. Soc. **130**, 6704 (2008).

- [13] G. W. Burr, B. N. Kurdi, J. C. Scott, C. H. Lam, K. Gopalakrishnan, et al., IBM J. Res. Dev. 52, 449 (2008).
- [14] M. Shisode, P. B. Kharat, D. N. Bhoyar, V. Vinayak, M. K. Babreka, et al., in: AIP Conference Proceedings, AIP Publishing, USA 2018.
- [15] J. Xie, C. Feng, X. Pan, and Y. Liu, Ceram. Int. 40, 703 (2014).
- [16] F. Gheorghiu, L. Curecheriu, A. Ianculescu, M. Calugaru, and L. Mitoseriu, Scr. Mater. 68, 305 (2013).
- [17] J. R. Sahu and C. Rao, Solid State Sci. 9, 950 (2007).
- [18] C. Yang, C. Z. Liu, C. M. Wang, W. G. Zhang, and J. S. Jiang, J. Magnetism Magnetic Mater. 324, 1483 (2012).
- [19] S. Rana and R. P. Singh, J. Mater. Sci. Mater. Electron. 27, 9346 (2016).
- [20] S. B. Rana, R. Singh, and S. Arya, J. Mater. Sci. Mater. Electron. 28, 2660 (2017).
- [21] R. P. P. Singh, I. S. Hudiara, S. Panday, and S. B. Rana, J. Superconduct. Novel Magnetism 29, 819 (2016).
- [22] M. Ahmad, R. Grössinger, I. Ali, I. Ahmad, and M. U. Rana, J. Alloys Comp. 577, 382 (2013).
- [23] A. Bhosale and B. Chougule, Mater. Chem. Phys. 97, 273 (2006).
- [24] M. Mozaffari, Z. Abooalizadeh, and J. Amighian, J. Magnetism Magnetic Mater. 323, 2997 (2011).
- [25] P. Kumar and M. Kar, Phys. B Condensed Matter 448, 90 (2014).
- [26] M. K. Sharif, M. A. Khan, A. Hussain, F. Igbal, I. Shakir, et al., J. Alloys Comp. 667, 329 (2016).
- [27] C. Ramesh, K. Maniysundar, and S. Selvanandan, Mater. Today Proc. 3, 1363 (2016).
- [28] V. Verma, A. Beniwal, A. Ohlan, and R. Tripathi, J. Magnetism Magnetic Mater. 394, 385 (2015).
- [29] V. Kumar, A. Gaur, N. Sharma, J. Shah, and R. K. Kotnala, Ceram. Int. 39, 8113 (2013).
- [30] A. Paul, M. J. H. van Dal, A. A. Kodentsov, and F. J. J. van Loo, Acta Mater. 52, 623 (2004).
- [31] M. W. Mukhtar, M. Irfan, I. Ahmad, I. Ali, M. N. Akhtar, et al., J. Magnetism Magnetic Mater. 381, 173 (2015).
- [32] K. Shehzad, M. Ahmad, C. Xie, D. Zhan, W. Wang, et al., J. Hazard. Mater. 373, 75 (2019).
- [33] F. Ren, H. Wang, P. A. Menchhofer, and J. O. Kiggans, Appl. Phys. Lett. 103, 221907 (2013).
- [34] G. F. Dionne, Proc. IEEE 63, 777 (1975).
- [35] J. Buban, Science 311, 212 (2006).
- [36] R. Mishra, D. K. Pradhan, R. N. P. Choudhary, and A. Banerjee, J. Phys. Condensed Matter 20, 045218 (2008).
- [37] W. Eerenstein, N. Mathur, and J. F. Scott, Nature 442, 759 (2006).
- [38] R. Mazumder, P. S. Devi, D. Bhattacharya, P. Choudhury, A. Sen, et al., Appl. Phys. Lett. 91, 062510 (2007).
- [39] T.-J. Park, G. C. Papaefthymiou, A. J. Viescas, A. R. Moodenbaugh, and S. S. Wong, Nano Lett. 7, 766 (2007).
- [40] P. Kumar and M. Kar, Mater. Chem. Phys. 148, 968 (2014).
- [41] J. Lin, Z. Guo, M. Li, Q. Lin, K. Huang, et al., J. Appl. Biomater. Funct. Mater. 16, 93 (2018).